Hindawi
Journal of Control Science and Engineering
Volume 2018, Article ID 1976836, 11 pages
https://doi.org/10.1155/2018/1976836

Research Article

Detection of Two-Level Inverter Open-Circuit Fault Using a Combined DWT-NN Approach

Bilal Djamal Eddine Cherif and Azeddine Bendiabdellah

Diagnostic Group, Laboratory LDEE, Electrical Engineering Faculty, University of Sciences and Technology of Oran, Bir El Djir, Algeria

Correspondence should be addressed to Bilal Djamal Eddine Cherif; cherif.doc84@gmail.com

Received 18 November 2017; Revised 19 January 2018; Accepted 29 January 2018; Published 11 March 2018

Academic Editor: Qiang Liu

Three-phase static converters with voltage structure are widely used in many industrial systems. In order to prevent the propagation of the fault to other components of the system and ensure continuity of service in the event of a failure of the converter, efficient and rapid methods of detection and localization must be implemented. This paper work addresses a diagnostic technique based on the discrete wavelet transform (DWT) algorithm and the approach of neural network (NN), for the detection of an inverter IGBT open-circuit switch fault. To illustrate the merits of the technique and validate the results, experimental tests are conducted using a built voltage inverter fed induction motor. The inverter is controlled by the SVM control strategy.

1. Introduction

Several researchers have carried out their investigation in relation to the field of detection and location of faults in static converters and more particularly those related to three-phase power inverters [1]. The treated fault is mainly concerned with the open-circuit fault of an inverter IGBT switch [2]. Most published papers are based on Park's current vectors approach [3]. This approach is based on the trajectory tracking of the phase current vector. In fact, for the case of a healthy state condition of the inverter, the trajectory of these current vectors in the (d-q) frame is a circle. It was found that the circle becomes a semicircle under an open-circuit IGBT switch fault in one of the legs of the inverter. The position of this semicircle in the (d-q) frame makes it possible to identify the faulty IGBT switch [4]. Another paper used the mean value of the phase currents in Park's frame for the extraction of the open-circuit fault angle of each IGBT switch [1–5]; unfortunately this method presents an inconvenience as it depends on the load. To overcome the problem, some authors suggested the normalized DC current method which is fundamentally based on the DC component of the current and the first-order harmonic coefficients of the alternating current (AC) [6]. Some detection techniques mentioned above are briefly discussed in [7, 8].

Others researchers used stator current as key parameter for fault diagnosis purpose because it does not require costly sensors. This technique is widely termed as Motor Current Signature Analysis (MCSA) technique [9–11]. For steady state constant load conditions, the Fast Fourier Transform (FFT) algorithm has been used for different induction motor fault diagnosis purpose. The (FFT) algorithm is able to diagnose bearing fault for full load conditions but not for the no-load or light load condition [7]. Therefore, some researchers proposed short-term Fourier transform (STFT) and wavelet transform (WT) methods for different fault diagnosis purpose of the induction motor by taking into consideration the quantity of time (that is for nonstationary applications). However, the (STFT) method faces a big disadvantage; it gives poor frequency resolution because it shows constant window size for all frequencies.

The wavelet transform (WT) technique has perhaps been the most persistent development in recent decades. It has drawn the attention of several researchers in various fields, such as signal processing, image processing, communication, computer science, and mathematics. Numerous works describing the advancement in wavelet theory and its applications in various fields have been published. Among others, it is one of the most attractive techniques in the field of

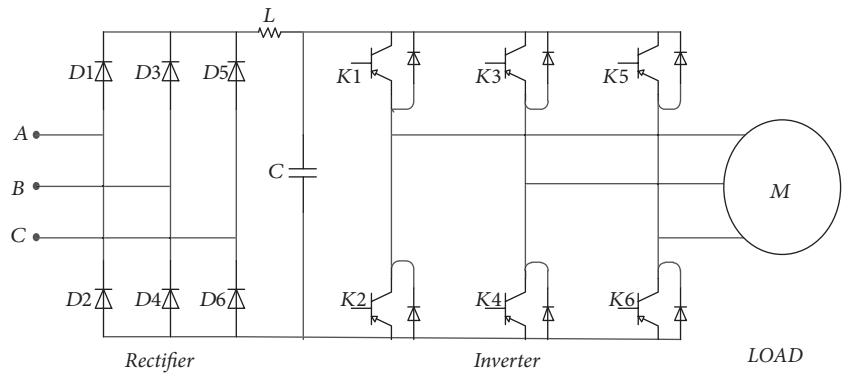

Figure 1: Structure of a three-phase two-level inverter.

rotary machines and static converter for fault diagnosis and it particularly matches well for the nonstationary signals [12, 13]. The main disadvantage of this technique is that the length of the range (scale) is fixed. Therefore, it is necessary to be able to keep the time-frequency representation and carry out an analysis based on a concept somewhat different from the concept of frequency: the scale concept [14]. In 1982, J. Morlet opens the way to the solution by constructing the wavelet analysis, based on the concept of scale. By manipulating the scale factor, one can zoom in and out a portion of the signal [14, 15]. Unlike the short-term Fourier transform, the wavelet transform uses the notion of time-scale involving dynamic length analysis windows. Because the continuous wavelet transform is very sensitive to noise, the discrete wavelet transform is preferred and used in our paper.

The application of artificial intelligence (AI) based techniques can be advantageous in fault diagnosis since these diagnoses have several advantages. For instance, since AI-based techniques do not require mathematical models, the development time can be significantly reduced. A literature review of recent developments in the field of AI-based diagnostic systems in power inverters has been presented [16]. In addition, some authors have studied the application of a neural network (NN) to establish a fault diagnosis system and judge the faults of power transistors [17]. These NN-based fault diagnosis methods allow an accurate solution to a particular fault problem without accurate knowledge of the faulty system. However, their main drawback is due to the fact that the exact architecture of the NN to be used is generally not known in advance.

The work proposed in this paper addresses an open-circuit fault detection of an IGBT switch of an inverter controlled by a DSPACE 1104 card based on the SVM control strategy feeding an induction motor. The analysis tools and fault diagnosis are based on the use of a combined DWT-NN approach. The DWT algorithm focuses on the investigation of the details of the stator current signal. The variation in these details for both healthy and faulty inverter cases enables us to extract useful information related to the open-circuit inverter switch faults. The NN approach is introduced in order to automate the fault diagnostic system by including a learning phase that helps in developing a very rich database storing relevant information about the open-circuit faults. To assess the effectiveness and merits of the proposed approach and validate the obtained results, experimental tests are conducted by the group diagnostic at the LDEE laboratory.

2. Voltage Source Inverter Structure

Figure 1 shows the structure of a three-phase two-level voltage source inverter feeding an induction motor.

This inverter is controlled by the SVM control strategy. For each leg of the inverter, there are two possible states:

(i) *State 1*: the higher switch K_X ($X = 1$, 2 or 3) is closed, while the lower switch K_X ($X = 1$, 2 or 3) is open. The output voltage relative to the neutral of the DC source is V_{dc}.

(ii) *State 0*: the lower switch K_X ($X = 1$, 2 or 3) is closed, while the higher switch K_X ($X = 1$, 2 or 3) is open. The output voltage relative to the neutral of the DC source is 0 v.

Unfortunately during its operation, various failures can affect the inverter especially in terms of its so-called power components (IGBT in our case study) because of their fragility. Two types of faults can be reported [1]:

(i) Short-circuit faults affecting the IGBT switches are the most serious faults. In the presence of such a fault, the current reaches limits which can cause the fusion of its chip or its connection. If the detection of this type of fault does not occur rapidly (less than 10 microseconds), then the IGBT switch which is still active on the same leg undergoes the same phenomenon and so the whole inverter leg is shorted.

(ii) Open-circuit faults affecting the IGBT switches may occur when, for any reason, the IGBT is disconnected, is damaged, or had a problem in its grid control signal. This type of fault is very difficult to perceive directly because the motor can continue to operate but with a degradation of its performance due to the occurrence of fluctuations in the mechanical parameters (speed and torque) as well as an imbalance of the currents where the currents of the other two healthy legs take high values to maintain the average torque and the

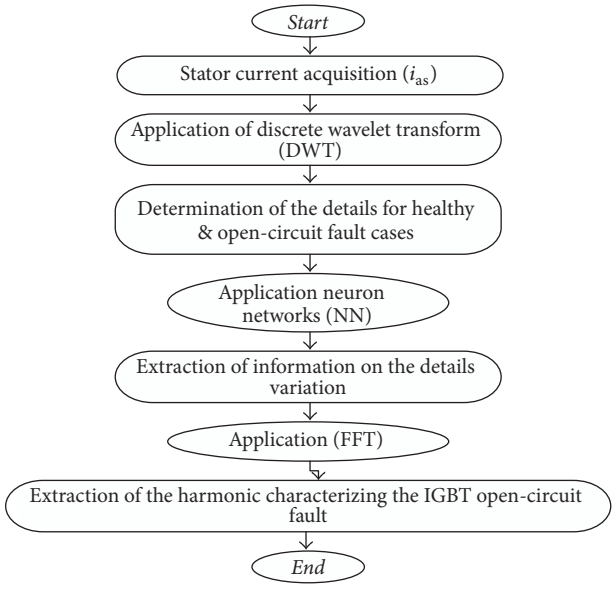

Figure 2: Flowchart of the proposed DWT-NN approach.

speed. The starting of the motor in the presence of this type of fault cannot always be ensured; everything will depend on the value of the torque which can be close to zero for certain rotor position.

3. Theoretical Bases of the Combined DWT-NN Approach

The flowchart presented in Figure 2 is to illustrate the main steps required when using the combined DWT-NN approach.

The following two subsections tackle in more detail both the DWT algorithm and the NN approach.

3.1. DWT Algorithm Principle. The wavelet transform is a mathematical tool which allows the decomposition of a temporal signal into a series of coefficients called approximation and detail; the approximations represent the slow variations of the signal, whereas the details represent the fastest [6, 7].

A wavelet $\psi(t)$ is an oscillating function of zero mean, with a certain degree of regularity and whose support is finite (which explains the word "wavelet," which means small wave). Mathematically, a wavelet $\psi(t)$ is a zero mean function that is expanded by a scale parameter and is translated by the time parameter b "translation in time parameter"; it is defined as follows:

$$\psi_{a,b}(t) = \frac{1}{\sqrt{a}}\Psi\left(\frac{t-b}{a}\right). \quad (1)$$

The expansions and translations of this "mother" wavelet are used to allow the projection of the signal over different time scales. These scales depend mainly on the sampling frequency F_e of the signal to be processed.

Under these conditions, a signal $x(t)$ can be represented as wavelets given by the following equation:

$$x(t) = \sum_{k=-\infty}^{\infty} c_k \varphi(t-k) + \sum_{k=-\infty}^{\infty}\sum_{j=0}^{\infty} d_{j,k} 2^{j/2} \psi\left(2^j t - k\right). \quad (2)$$

$\psi(t)$ is the derivative of the function $\varphi(t)$ with

$$c_k = \int_{-\infty}^{\infty} x(t)\,\varphi(t-k)\,dt,$$
$$d_{j,k} = \int_{-\infty}^{\infty} x(t)\,2^{j/2}\psi\left(2^j t - k\right)dt, \quad (3)$$

where c_k are called the approximation coefficients and $d_{j,k}$ the detail coefficients.

In the case of a discrete wavelet transform (DWT) which is the tool of our paper work, the expansion and translation parameters "a" and "b" of $\psi(t)$ are limited only to discrete values leading to the following expression:

$$\psi_{m,n}(t) = \frac{1}{\sqrt{a_0^m}}\psi\left(\frac{t - nb_0a_0^m}{a_0^m}\right), \quad (4)$$

where the parameters "m" and "n" are integers allowing the control of the dilation and the translation of the mother wavelets

Obviously, according to the last equation, different wavelets (Haar, Daubechies, Coiflet, Meyer, Morlet, etc.) generate different wavelet classes and consequently the behavior of the decomposed signal can be very different. In fact, each wavelet has particular characteristics whose choice depends on the desired application. In this paper, the Coiflet wavelets are to be applied for the detection of the IGBT open-circuit. Figure 3 depicts a typical Coiflet wavelet family graphical representation.

3.1.1. Number of Decomposition Levels Required. The DWT using the Coiflet algorithm is based on signal the decomposition using low-pass filters (LPF) and high-pass filters (HPF) followed by subsampling. Then, in each level of decomposition, the coefficients of approximation and details are computed. Figure 4 shows the implementation of the DWT for three decomposition levels as an example.

Where the LPF frequency band is defined as

$$\left[0 \;\; \frac{Fe}{2^n}\right], \quad n = 1, 2, \ldots, N\text{levels}. \quad (5)$$

And the HPF frequency band is defined as

$$\left[\frac{Fe}{2^n}, \frac{Fe}{2^{(n-1)}}\right], \quad n = 1, 2, \ldots, N\text{levels}, \quad (6)$$

where n indicates the number of decomposition levels and the Nlevels are the maximum number of decomposition levels.

Prior knowledge of N_{levels} of the signal to be processed is essential for a reliable and fast analysis by the Coiflet mother wavelet. The following equation gives this required parameter [11]:

$$N_{\text{levels}} = \text{int}\left(\frac{\log(F_e/f_s)}{\log(2)}\right) + 2, \quad (7)$$

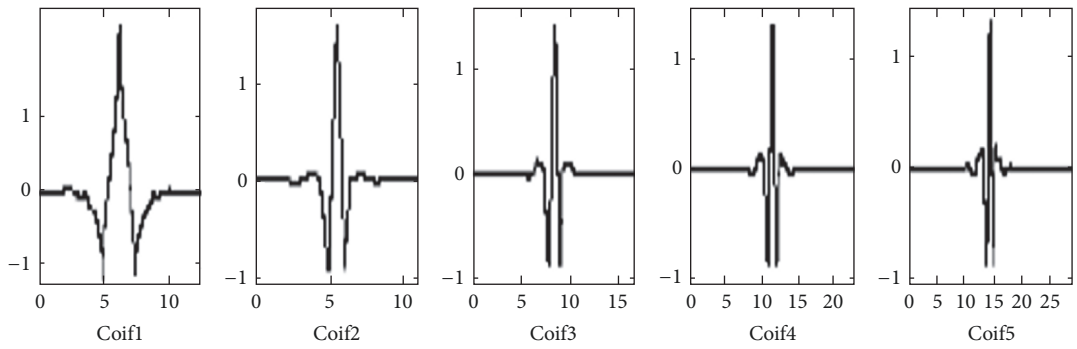

Figure 3: Coiflet wavelet families [16].

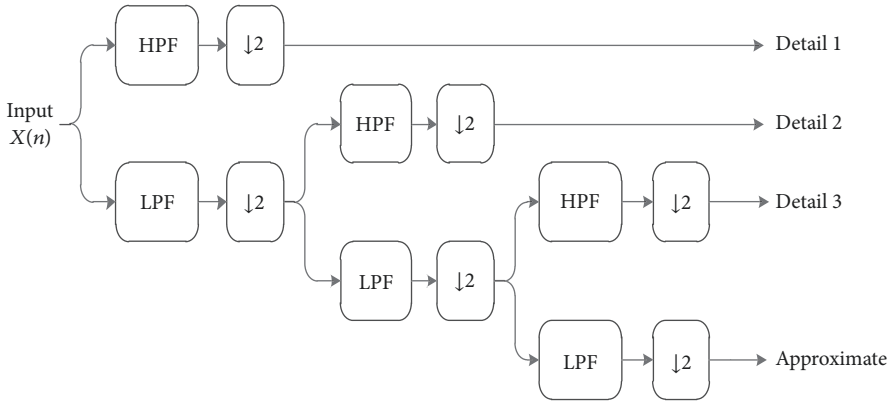

Figure 4: DWT implementation procedure.

where f_s is the supply frequency and F_e is the sampling frequency. Note that N_{levels} must obviously be an integer.

Knowing f_s and F_e, one can calculate the number of appropriate decompositions. For our case paper study, considering a sampling frequency of 1500 Hz and a supply frequency of 50 Hz, the number of decomposition levels required is

$$N_{\text{levels}} = \text{int}\left(\frac{\log(1500/50)}{\log(2)}\right) + 2 = \text{int}(4.9068) + 2 = 6 \text{ levels}. \quad (8)$$

Using (5) and (6) and the number of levels computed from (8), the decomposition of the motor stator current signal as a function of the sampling frequency for the six levels of decomposition can thus be obtained as illustrated in Figure 5.

3.2. Description of the Neural Network Approach. The proposed NN is a multilayer network of (6-6-1) whose adopted architecture is illustrated in Figures 6 and 7. Note that the smallest error is obtained after 38 iterations.

Each neuron is connected to all the neurons of the next layer by connections whose weights are any real numbers.

The neuron network study used in this paper is carried out through the three main steps:

(i) The construction of the network NN block using the Levenberg algorithm

(ii) The data acquisition (learning base)

(iii) The network test

3.3. Construction of the NN Block System. Figure 6 shows that our network consists of three layers:

(i) An input layer composed of six neurons, whose role is to transmit the values of the inputs that correspond to the maxima of details (max($d1$), max($d2$), max($d3$), max($d4$), max($d5$), and max($d6$)) to the next layer, called hidden layer

(ii) A hidden layer with six neurons with selected sigmoid activation functions

(iii) An output layer, which is composed of a neuron, where output of each neuron is 0 or 1

3.4. Acquisition of the Data (Learning Basis). Before building the NN block system, one must first access the learning phase. This can be in the form of a table. The latter consists of vectors (which represent the input layer of the NN), where each vector consists of 2 parameters.

A very rich database for healthy and faulty (open-circuit) cases can be developed, which has a lot of information about the open-circuit fault. During this phase, the maxima details of the healthy case are taken as the references; then the maxima of details for the faulty case are extracted and

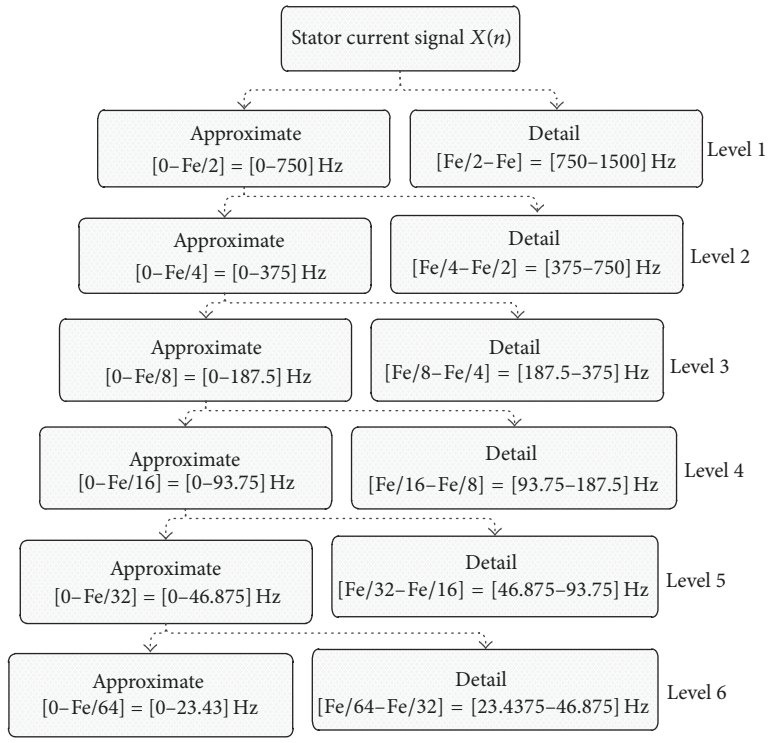

Figure 5: Decomposition of stator current signal $x(t)$.

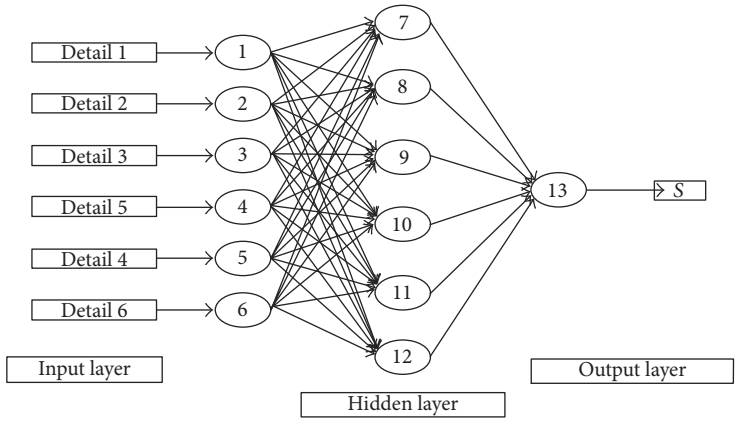

Figure 6: Proposed neural network architecture.

Table 1: Fault classification.

State	Fault type	Symbol	Code
1	Healthy state	HS	0
2	Open-circuit at K_1	OC	1

compared with the healthy case. From this comparison, it can be deduced as either state 0 (i.e., no variation in detail) or state 1 (i.e., variation in detail). Table 1 is to resume the task of this phase.

3.5. Network Test Results. An automatic learning was performed using the MATLAB software. The learning is reached once a small quadratic error of value $2.2181e^{-16}$ is obtained; see Figure 7. Note that the smallest error is obtained after 38 iterations.

4. Experimental Test-Rig

4.1. Experimental Test-Rig Description. The experimental test-rig used in this paper work includes a three-phase induction squirrel-cage motor fed by a three-phase two-level voltage source inverter. The detailed characteristics of the motor are given in the Appendix. Furthermore, the motor is mechanically coupled to a DC generator supplying resistors which allows varying the load torque. Moreover, the

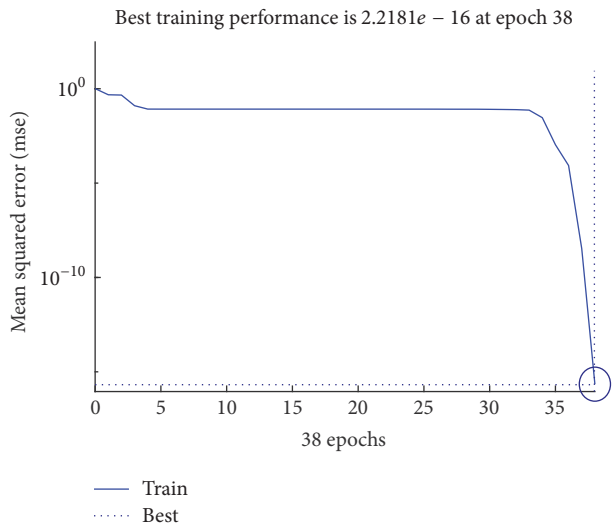

FIGURE 7: Evaluation of the quadratic error as a function of the number of learning iterations (using the method of retrogradient propagation).

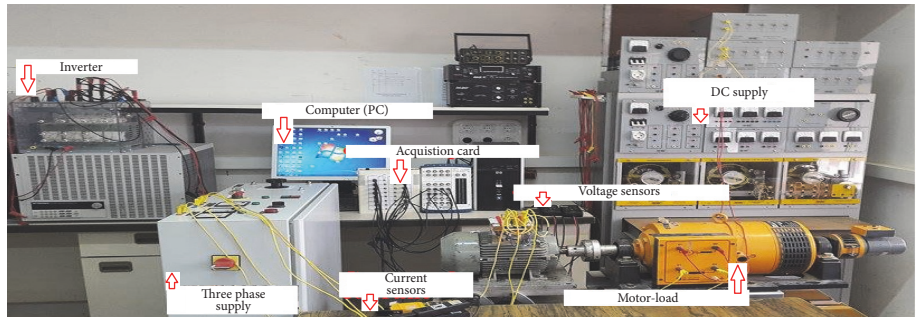

FIGURE 8: Photo of the experimental test-rig.

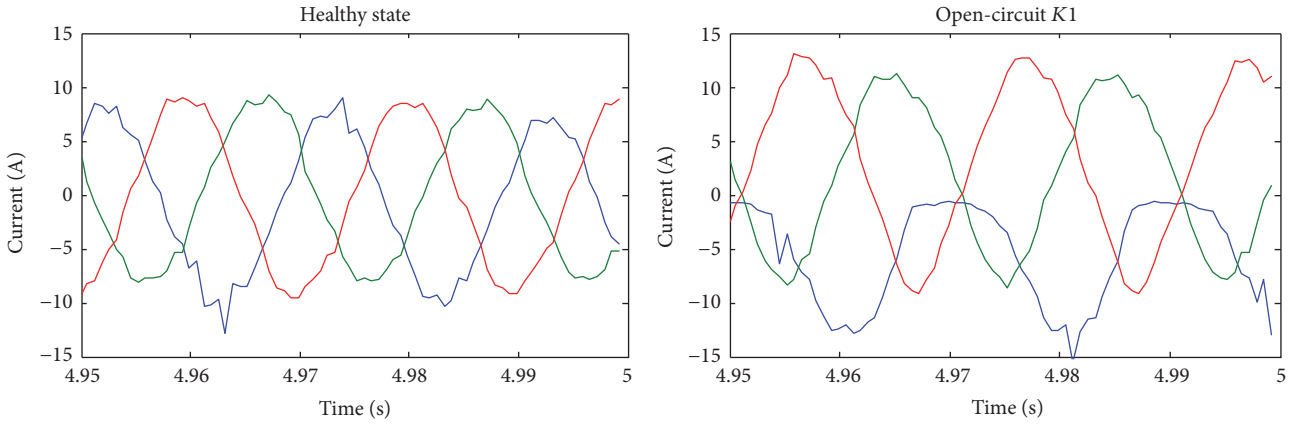

FIGURE 9: Currents waveforms of an induction motor for healthy and faulty open-circuit K_1 case.

measuring system includes three current Hall effect sensors and three voltage sensors and a DSPACE 1104 acquisition card to generate pulses for triggering the IGBTs gates. The whole set is connected to a computer for visualizing the processed sensed signal as shown in the photo of Figure 8. The acquisition time is taken as $T\text{acq} = 5$ s and the sampling frequency $Fe = 1500$ Hz.

4.2. Experimental Results Presentation and Discussion. Figure 9 depicts the phase current waveforms of the induction motor for both a healthy state and an IGBT open-circuit faulty inverter.

From the experimental results depicting the currents waveforms of the motor in Figure 9, following an IGBT open-circuit fault K_1 of the inverter leg, the phase current

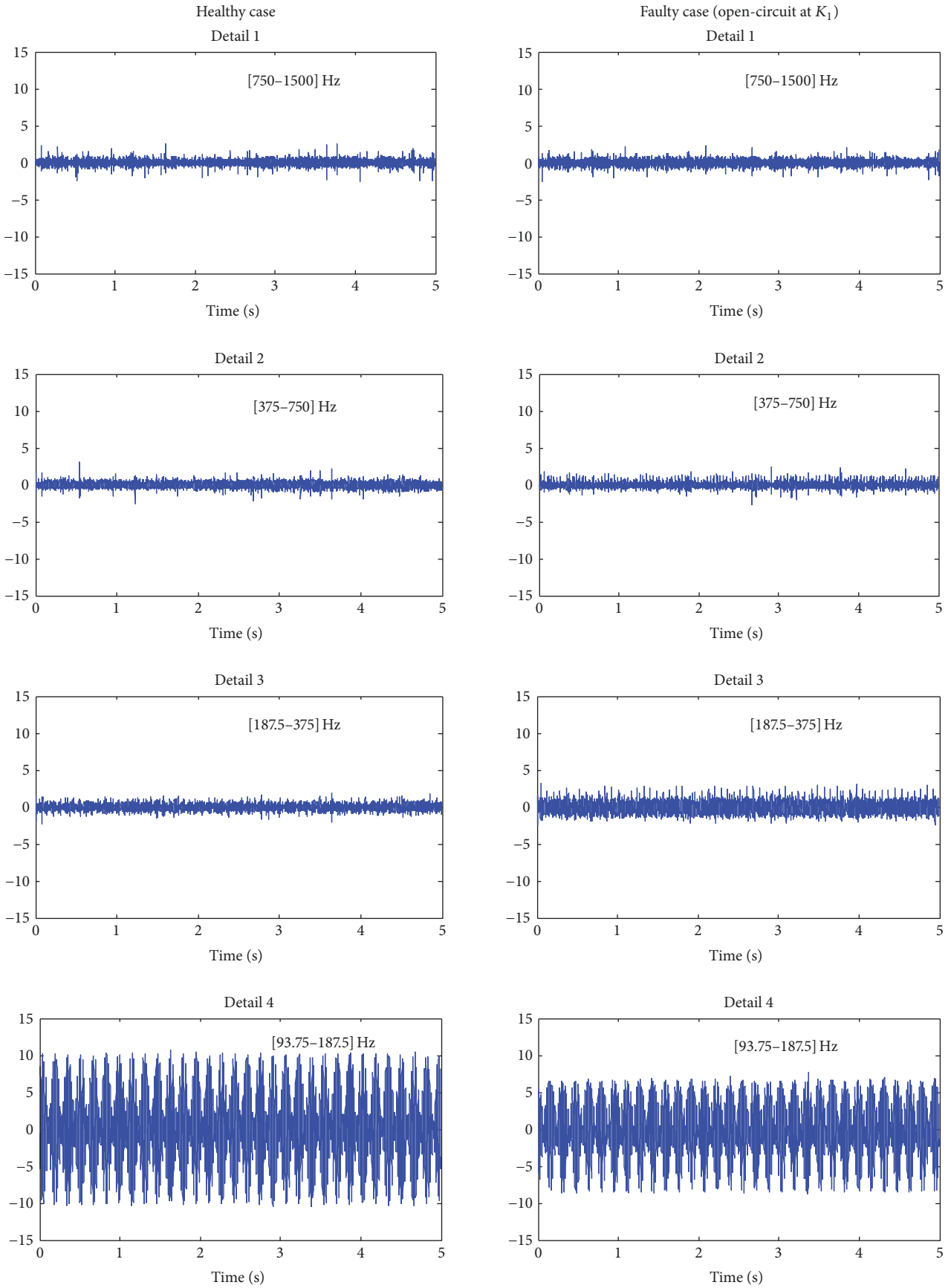

Figure 10: Continued.

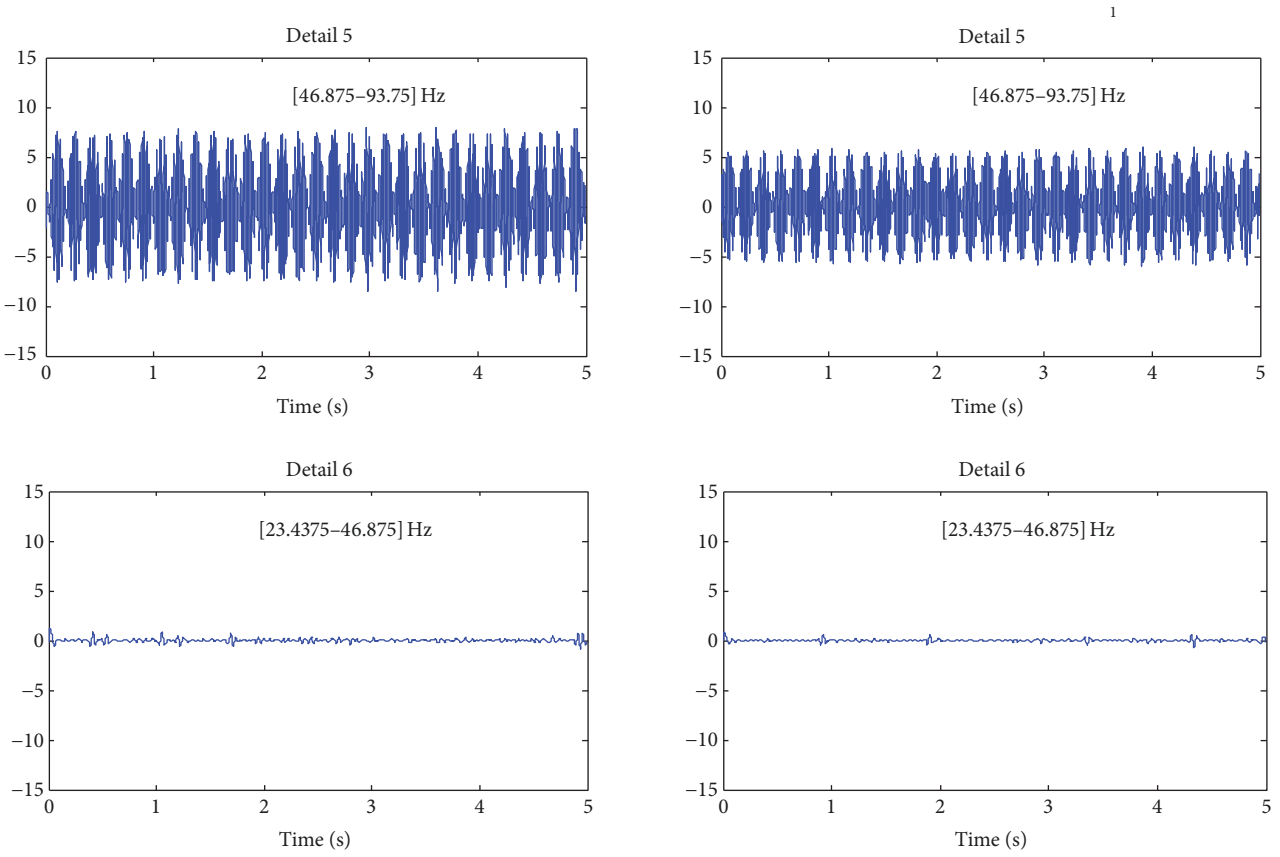

Figure 10: Details signal decomposition for healthy and faulty open-circuit at K_1 cases.

connected to this leg can no longer be controlled as it can only be negative or zero. The sum of the currents of the other two healthy phases is zero which may make it impossible to start the motor or to ensure for long term the continuity of service of the motor.

Figure 10 shows the various details extracted from the acquired stator current signal using the DWT technique for the healthy case and the faulty (open-circuit switch at K_1) case.

Figure 11 depicts the fault diagnostic system and Table 2 shows some examples of the diagnostic results.

Table 2 presents the input and output of the NN.

By comparing the details for the case of the healthy inverter state and that of the open-circuit switch fault state as depicted in Figure 11 or Table 2, a noticeable change in the amplitude of both details $d3$, $d4$ is easily observed, while the rest of the details remain almost the same independently of the open-circuit switch fault presence or not. The change in these two details $d3$ and $d4$ indicates the existence of certain information within our stator current signal. To extract and explain this information, a stator current spectral analysis based on the FFT is performed for both details.

Figure 12 presents the spectra of the frequency ranges $d3$: [187.5–375] and $d4$: [93.75–187.5] for the healthy and the faulty cases, respectively.

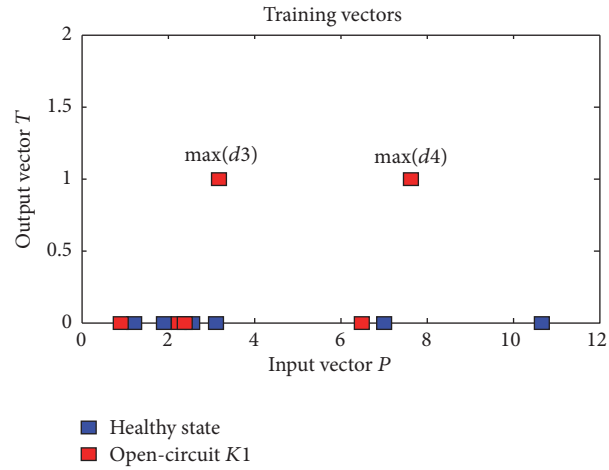

Figure 11: Variation of the details maxima.

Comparing both spectra in Figure 12 for healthy state and open-circuit fault state, we can easily notice the presence of additional harmonics characterizing the inverter open-circuit fault at frequencies 100 Hz in the first band [93.75–187.5] and 200 Hz and 300 Hz in the second band [187.5–375]. The amplitude and frequency of the various

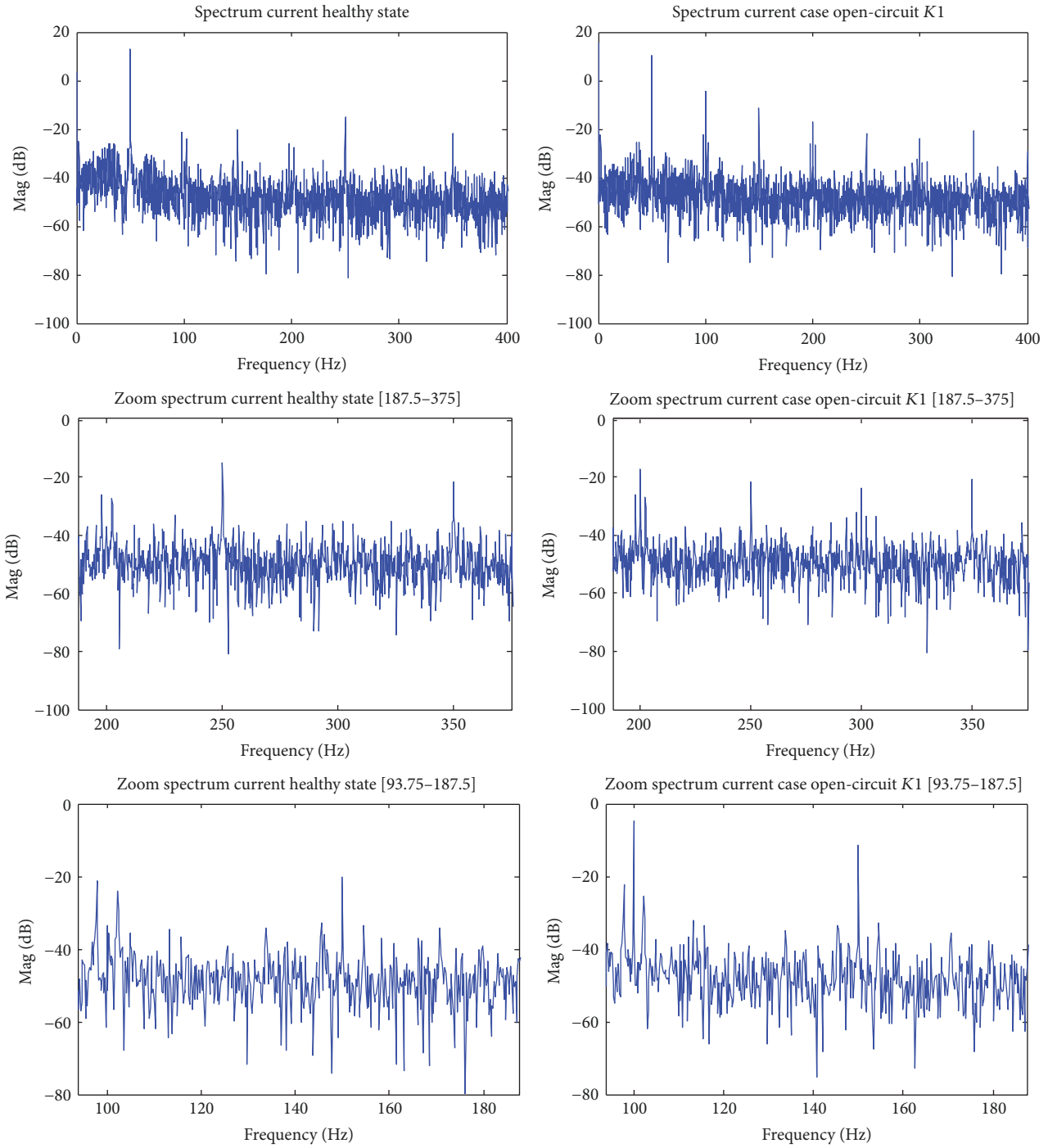

Figure 12: FFT of stator current signal for healthy and faulty open-circuit at K_1 cases.

Table 2: Details of one stator current phase for both healthy and faulty open-circuit at K_1 cases.

Max details	max(d_1)	max(d_2)	max(d_3)	max(d_4)	max(d_5)	max(d_6)
Input						
Healthy state	2.568	3.126	1.928	10.67	7.014	1.228
Open-circuit state K_1	2.261	2.412	3.206	7.632	6.502	0.909
Output	−0.0000	0.0000	1.0000	1.0000	0.0000	0.0000

Table 3: Amplitudes and frequencies of harmonics.

Harmonic (Hz)	$f_{oc} = 2f_s =$ 100 Hz	$4f_s = 200$ Hz	$6f_s = 300$ Hz
Healthy state (db)	−33.51 db	−37.25 db	0 db
Open-circuit state (db)	−4.623 db	−17.26 db	−23.77 db

obtained harmonics for the healthy and faulty cases are summarized in Table 3.

A comparative analysis between both healthy and faulty states shows with more clarity a particular frequency signature around 100 Hz for the spectrum level $d3$. Note that the open-circuit frequency $f_{oc} = 2f_s = 100$ Hz corresponds to the harmonic frequency that characterizes the open-circuit fault of the IGBT switch.

5. Conclusion

In this paper, a research area dealing with the technique of diagnosis and detection of open-circuit fault in a three-phase two-level voltage source inverter fed induction motor is investigated. The paper proposes a diagnosis approach based on the association of both the discrete wavelet transform (DWT) and the neural network (NN) for the detection of the IGBT open-circuit fault of an inverter.

The study focuses first on the extraction of the details for the cases of the healthy and the open-circuit faulty IGBT by using the DWT algorithm. The investigation of the harmonics related to the obtained details particularly $d3$ and $d4$ is then conducted by using the FFT technique. The NN enables the development of a rich database for both healthy and faulty cases resulting in the automation of the diagnostic system.

The various obtained results are validated by several experimental tests conducted in the LDEE laboratory by the group diagnostic to assess the effectiveness and merits of the combined DWT-NN proposed approach.

Appendix

Rated power: 3 KW

Supply frequency: 50 Hz

Rated voltage: 380 V

Rated current: 7 A

Rotor speed: 1440 rev/min

Number of rotor bars: 28

Number of stator slots: 36

Power factor: 0.83

Number of pair of poles: 2

Conflicts of Interest

The authors declare that there are no conflicts of interest regarding the publication of this paper.

References

[1] W. Zhang, D. Xu, P. N. Enjeti, H. Li, J. T. Hawke, and H. S. Krishnamoorthy, "Survey on fault-tolerant techniques for power electronic converters," *IEEE Transactions on Power Electronics*, vol. 29, no. 12, pp. 6319–6331, 2014.

[2] T. Orlowska-Kowalska and P. Sobanski, "Simple diagnostic technique of a single IGBT open-circuit faults for a SVM-VSI vector controlled induction motor drive," *Bulletin of the Polish Academy of Sciences—Technical Sciences*, vol. 63, no. 1, pp. 281–288, 2015.

[3] B. D. E. Cherif, A. Bendiabdellah, and M. A. Khelif, "Detection of open-circuit fault in a three-phase voltage inverter fed induction motor," *International Review of Automatic Control*, vol. 9, no. 6, pp. 374–382, 2016.

[4] B. D. E. Cherif, M. Bendjebbar, N. Benouzza, H. Boudinar, and A. Bendiabdellah, "A comparative study between two open-circuit fault detection and localization techniques in a threephase inverter fed induction motor," in *Proceedings of the 2016 8th International Conference on Modelling, Identification and Control (ICMIC)*, pp. 1–7, Algiers, November 2016.

[5] H. Keskes, A. Braham, and Z. Lachiri, "Broken rotor bar diagnosis in induction machines through stationary wavelet packet transform and multiclass wavelet SVM," *Electric Power Systems Research*, vol. 97, pp. 151–157, 2013.

[6] R. Yan, R. X. Gao, and X. Chen, "Wavelets for fault diagnosis of rotary machines: a review with applications," *Signal Processing*, vol. 96, pp. 1–15, 2013.

[7] A. F. Aimer, A. H. Boudinar, N. Benouzza, and A. Bendiabdellah, "Simulation and experimental study of induction motor broken rotor bars fault diagnosis using stator current spectrogram," in *Proceedings of the 3rd International Conference on Control, Engineering and Information Technology, CEIT 2015*, dza, May 2015.

[8] Z. Liu, Y. Cui, and W. Li, "Combined power quality disturbances recognition using wavelet packet entropies and S-transform," *Entropy*, vol. 17, no. 8, pp. 5811–5828, 2015.

[9] Q. Yang and J. Wang, "Multi-level wavelet shannon entropy-based method for single-sensor fault location," *Entropy*, vol. 17, no. 10, pp. 7101–7117, 2015.

[10] S. Kaur, K. Gaganpreet, and S. Dheerendra, "Comparative analysis of haar and coiflet wavelets using discrete wavelet transform in digital image compression," *International Journal of Computer Applications (IJERA)*, vol. 3, no. 3, pp. 669–673, 2013.

[11] J. A. Antonino-Daviu, M. Riera-Guasp, J. R. Folch, and M. P. Molina Palomares, "Validation of a new method for the diagnosis of rotor bar failures via wavelet transform in industrial induction machines," *IEEE Transactions on Industry Applications*, vol. 42, no. 4, pp. 990–996, 2006.

[12] R. R. Errabelli and P. Mutschler, "Fault-tolerant voltage source inverter for permanent magnet drives," *IEEE Transactions on Power Electronics*, vol. 27, no. 2, pp. 500–508, 2012.

[13] T. Orlowska-Kowalska and P. Sobanski, "Simple sensorless diagnosis method for open-switch faults in SVM-VSI-fed induction motor drive," in *Proceedings of the 39th Annual Conference of the IEEE Industrial Electronics Society, IECON 2013*, pp. 8210–8215, Austria, November 2013.

[14] W.-S. Im, J.-S. Kim, J.-M. Kim, D.-C. Lee, and K.-B. Lee, "Diagnosis methods for IGBT open switch fault applied to 3-phase AC/DC PWM converter," *Journal of Power Electronics*, vol. 12, no. 1, pp. 120–127, 2012.

[15] I. Jlassi, S. Khojet, and E. Khil, "A MRAS-Luenberger observer based fault tolerant control of PMSM drive," *Journal of Electrical Systems*, vol. 10, no. 1, pp. 48–62, 2014.

[16] B. Fan, Y. Yin, and C. Fu, "A method of inverter circuit fault diagnosis based on BP neural network and D-S evidence theory," in *Proceedings of the 2010 8th World Congress on Intelligent Control and Automation, WCICA 2010*, pp. 2249–2253, China, July 2010.

[17] L. hong and W. yan-qiu, "Study of Fault Diagnosis on Three-phase Sine-PWM Inverter Based on Rough Set-neural Network System," *Journal of Liaoning Istitute of Technology*, vol. 25, no. 6, pp. 351–353, 2005.